Taylor & Francis
Taylor & Francis Group

A new flat shell finite element for the linear analysis of thin shell structures

Djamal Hamadi[a], Ashraf Ayoub[b] and Ounis Abdelhafid[a]

[a]Faculty of Sciences and Technology, Civil Engineering and Hydraulics Department, Biskra University, Biskra, Algeria; [b]School of Mathematics, Computer Science, and Engineering, City University London, London, UK

ABSTRACT

In this paper, a new rectangular flat shell element denoted 'ACM_RSBE5' is presented. The new element is obtained by superposition of the new strain-based membrane element 'RSBE5' and the well-known plate bending element 'ACM'. The element can be used for the analysis of any type of thin shell structures, even if the geometry is irregular. Comparison with other types of shell elements is performed using a series of standard test problems. A correlation study with an experimentally tested aluminium shell is also conducted. The new shell element proved to have a fast rate of convergence and to provide accurate results.

1. Introduction

Analytical solutions of practical thin shell structures, particularly those with irregular geometrical shapes, are complex and thus a resort to numerical methods when analysing them becomes essential. Early work aimed to study shells of revolution in which closed ring shell segments are used (e.g. Jones & Strome, 1966). The formulation of flat elements (Zienkiewics, 1977) and curved rectangular elements (Corner & Brebbia, 1967) followed. These elements are based on assumed polynomial displacements with linear representation of the in-plane displacements. These elements were found to have a slow rate of convergence, thus the development of high-order elements received more attention. Meanwhile, a simple strain-based alternative approach was proposed by Ashwell and Sabir (1972). In this approach, the exact terms representing all rigid body modes and displacement functions corresponding to the element strains are determined by assuming independent strain functions that satisfy the compatibility equations. This approach was used successfully by Sabir and his co-workers (1982, 1985, 1990,

CONTACT Ashraf Ayoub ✉ Ashraf.Ayoub.1@city.ac.uk

1997) and Mousa and Sabir (1994) to analyse cylindrical, hyperbolic and conical shell structures. These elements in general proved to have a faster convergence rate compared to other models available in the literature. On the other hand, a family of enhanced strain elements, originally developed by Simo and Rifai (1990), were proposed. These include one-point quadrature elements developed by Cardoso, Yoon, and Valente (2006); Cardoso et al. (2008), four-node exact geometry element proposed by Kulikov and Plotnikova (2010), the improved solid–shell elements of Abed-Meraim and Combescure (2009) using physical stabilisation, of Reese (2007) using hourglass stabilisation and of Schwarze and Reese (2009) using reduced integration.

The proposed strain-based approach was also used to develop rectangular and triangular spherical shell elements with five degrees of freedom at each node by Sabir and Djoudi (1998) and Mousa (1992), respectively. These spherical elements were found to produce excellent results with a fast convergence rate. Recently, this approach, also known as the Cardiff Approach, was employed to develop several shell elements, most notably the shallow shell finite element for the analysis of cylindrical shells as well as the cylindrical strain-based shell element for vibration analysis of shell structures developed by Djoudi and Bahai (2003, 2004), respectively. The results of these elements show that efficient convergence can be obtained. More recently, a spherical rectangular finite element based on shallow shell formulation was formulated by Mousa and EL Naggar (2007). This element has six degrees of freedom at each node and proved to yield accurate results even when using very few finite elements. We note here that most of the above efficient elements are formulated with the appropriate coordinates of the geometrical shape of the structures. Generally, for design purposes, shell structures are constructed with very complicated geometrical shapes and elements, such as folded plates and edge beams. Additional geometrical problems arise such as when openings, anisotropy or variation of thickness are present. However, for practical purposes the flat element approximation gives generally adequate results and permits easy coupling with edge beams and rib members, a capability usually not present in curved element formulations (Zienkiewics & Taylor, 2000). In flat shell elements, the coupling between membrane and bending action is accounted for at the integration points due to the varying orientation of the element. For practical analysis of shell structures, such flat plate element assumption is typically acceptable, and has the advantage of ease of modelling with reasonable accuracy. Further, because the membrane and bending stresses within an element are decoupled it is easy to understand and control the behaviour of such elements (Hartmann & Kats, 2007). In this case, the behaviour of a continuously curved surface is represented by a surface made up of small flat elements. Intuitively, as the size of the subdivision decreases it would seem that convergence must occur as discussed by Zienkiewics and Taylor (2000).

In this paper, a new flat shell element is proposed and is denoted as (ACM_RSBE5). The element is developed by superposition of the new rectangular

membrane element R4SBE5 based on the strain approach and the well-known plate bending element ACM discussed in detail in Adini and Clough (1961) and Melosh (1963). The element is characterised by its simplicity compared to existing elements, without compromising its numerical robustness. The stiffness matrix of the new shell element is obtained by combining the two independent membranes and bending stiffness matrices. The displacement field for the strain-based membrane element RSBE5 used to construct the flat shell element fully satisfies the equilibrium equations in addition to the compatibility equations. Also, the technique of static condensation of a middle node and the new analytical integration employed in the formulation are the new additions that distinguish this element from other flat shell elements presented in previously published works (e.g. Ashwell & Sabir, 1972; Sabir & Lock, 1972; Belarbi, 2000; Batoz & Dhatt, 1992].

Ashwell and Sabir (1972) developed a cylindrical shell finite element. The element is a rectangular one, having 20 degrees of freedom. It uses only external geometrical nodal displacement, three linear displacements and two rotations; and its formulation is based on strain functions using polar coordinates. The effectiveness of this element has been tested by using it for the analysis of pinched cylinder shell and barrel vault problems. The results showed rapid convergence for displacement. Sabir and Lock (1972) also developed a curved cylindrical shell finite element. They used the standard finite-element approach for the formulation adopted by Cantin and Clough (1968), but removed the nodal degrees w_{xy} and included terms containing trigonometrical functions to develop a rectangular cylindrical shell element with four nodes and five dof/node, which leads to a 20×20 element stiffness matrix. This element is found to converge more rapidly than the Cantin and Clough's model for both symmetrical and unsymmetrical loading conditions. The applications of the elements developed by Sabir and his co-workers are limited to cylindrical shell structures, while the proposed element is a flat shell which can be used for the analysis of general shape shell structures. The present element contains a middle node to enrich the displacement field that is subsequently condensed out. The element also uses an analytical integration to evaluate the stiffness matrix.

Belarbi (2000) formulated a flat quadrilateral shell element named ACM-SBQ4, obtained by superimposing the standard membrane element SBQ4 with the plate bending element ACM (Melosh, 1963). The SBQ4 element (Strain Based Quadrilateral element with 4-node) is based on the strain approach, with three degrees of freedom per node including a drilling rotation. The membrane and bending stiffness matrix is obtained by using an analytical integration. This element was examined with three essential shell tests and the results obtained are compared with those of the proposed ACM_RSBE5 in addition to the reference solution. The membrane element SBQ4 contains four nodes and three DOF/node (2 translations and one drilling rotation), but the present element RSBE5 contains five nodes: four corner nodes and a middle node with two translations/node.
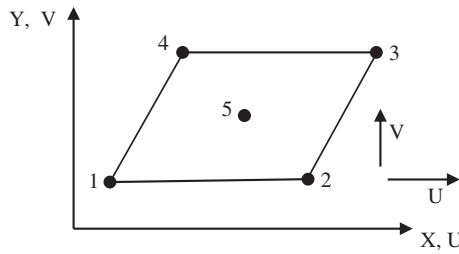
Figure 1. Co-ordinates and nodal points for the rectangular element 'RSBE5'.

Batoz and Dhatt (1992) formulated a set of quadrilateral shell elements based on displacement formulations, among them Q4γ24 and DKQ24. The first element is based on the Mindlin theory formulation, having four nodes with six degrees of freedom per node and using numerical integration. The second is a flat shell element obtained by superposition of the well-known classical quadrilateral membrane element Q4 and the plate bending element DKQ (Discrete Kirchhoff quadrilateral element with 4 nodes and 3 dof per node). The DKQ24 element is based on the Kirchhoff theory with four nodes and six degrees of freedom per node. These two elements are applied to the numerical analysis of Scordelis and Lo (1969) roof test presented in the numerical section in this paper. The results obtained are compared with the reference solutions for both shallow and deep shell theory, in addition to the new formulated element 'ACM_RSBE5' and the flat shell element ACM-SBQ4. We should mention here that the analytical integration technique is used to compute the element stiffness matrices for both elements 'ACM_RSBE5' and ACM-SBQ4. The improved results obtained from the numerical simulations clearly prove the advantages of the proposed element.

In the next section, the formulation of the new element ACM_RSBE5 is presented, followed by standard test problems to evaluate its convergence compared to other quadrilateral shell elements present in the literature. Finally, a correlation study with an experimentally tested elliptical paraboloid shell structure subjected to a uniformly distributed load is presented and the results are discussed.

2. Construction of the new flat shell element ACM_RSBE5

The proposed rectangular shell element is obtained by the superposition of the new formulated element 'RSBE5' based on the strain approach and described in the next section, and the **ACM** standard plate bending element. The stiffness matrix of the shell element **ACM_ RSBE5** is calculated through the analytical integration of the membrane and bending stiffness matrices.

2.1. Formulation of the new membrane element 'RSBE5'

Figure 1 shows the geometry and nodal displacements of the 'RSBE5' element (*Rectangular Strain Based Element with 5 nodes)*. The degrees of freedom at each node (i) are denoted U_i and V_i for the horizontal and vertical displacements, respectively. The element was developed by Hamadi (2006) and has four nodes at the corner in addition to an internal node, each having two degrees of freedom (d.o.f). Through the introduction of an additional internal node, the element has proven to be more accurate, even though it requires static condensation following the approach of Bathe and Wilson (1976).

The strain components at any point in the Cartesian coordinate system are expressed in terms of the displacements U and V as follow:

$$\varepsilon_x = U,_x \tag{1a}$$

$$\varepsilon_y = V,_y \tag{1b}$$

$$\gamma_{xy} = U,_y + V,_x \tag{1c}$$

If the strains given by equations (1) are equal to zero, the integration of equations (1) leads to expressions of the form:

$$U = a_1 - a_3\, y \tag{2a}$$

$$V = a_2 + a_3\, x \tag{2b}$$

Equations (2) represent the displacement field in terms of its three rigid body displacements. The strains in Equation (1) cannot be considered independent since they must satisfy the compatibility equation. This equation can be obtained by eliminating U, V from Equation (1), hence:

$$\frac{\partial^2 \varepsilon_x}{\partial y^2} + \frac{\partial^2 \varepsilon_y}{\partial x^2} - \frac{\partial^2 \gamma_{xy}}{\partial x \partial y} = 0 \tag{3}$$

Equation (2) represents the three components of the rigid body displacements through three independent constants (a_1, a_2, a_3). Thus, seven additional constants $(a_4, a_5 \ldots a_{10})$ are needed to express the displacements due to straining of the element. These seven independent constants are used to describe the strains as follow:

$$\begin{cases} \varepsilon_x = a_4 + a_5 y + a_9 x \\ \varepsilon_y = a_6 + a_7 x + a_{10} y \\ \gamma_{xy} = -a_5 x R - a_7 y R + a_8 - a_9 H y - a_{10} H x \end{cases} \quad (4)$$

With: $H = \frac{2}{(1-v)}; R = \frac{2v}{(1-v)}$

The strains given by equations (4) satisfy both the compatibility equation (3) and the two-dimensional equilibrium Equations (5a) and (5b):

$$\frac{\partial \sigma_x}{\partial x} + \frac{\partial \tau_{xy}}{\partial y} = 0 \quad (5a)$$

$$\frac{\partial \sigma_y}{\partial y} + \frac{\partial \tau_{xy}}{\partial x} = 0 \quad (5b)$$

By integrating equations (4), the displacements are evaluated as follow:

$$U = a_4 x + a_5 xy - a_7 y^2 (R + 1)/2 + a_8 y/2 + a_9 \left(x^2 - H y^2\right)/2 \quad (6a)$$

$$V = - a_5 x^2 (R + 1)/2 + a_6 y + a_7 xy + a_8 x/2 + a_{10}\left(y^2 - Hx^2\right)/2 \quad (6b)$$

By adding Equations (2) and (6), the final displacements representing rigid body modes and straining actions are evaluated as follow:

$$\begin{cases} U = a_1 - a_3 y + a_4 x + a_5 xy - a_7 \dfrac{y^2(R+1)}{2} + a_8 \dfrac{y}{2} + a_9 \dfrac{1}{2}(x^2 - Hy^2) \\ V = a_2 + a_3 x - a_5 \dfrac{x^2(R+1)}{2} + a_6 y + a_7 xy + a_8 \dfrac{x}{2} + a_{10}\dfrac{1}{2}(y^2 - Hx^2) \end{cases} \quad (7)$$

The stiffness matrix is then calculated from the well-known expression:

$$\left[K_e\right] = \left[A^{-1}\right]^T \left[K_0\right] \left[A^{-1}\right] \quad (8a)$$

where

$$\left[K_0\right] = \iint_S [Q]^T [D][Q] dx.dy \quad (8b)$$

and

$$[Q] = \begin{bmatrix} 0 & 0 & 0 & 1 & y & 0 & 0 & 0 & x & 0 \\ 0 & 0 & 0 & 0 & 0 & 1 & x & 0 & 0 & y \\ 0 & 0 & 0 & 0 & -xR & 0 & -yR & 1 & -Hy & -Hx \end{bmatrix} \quad (9)$$
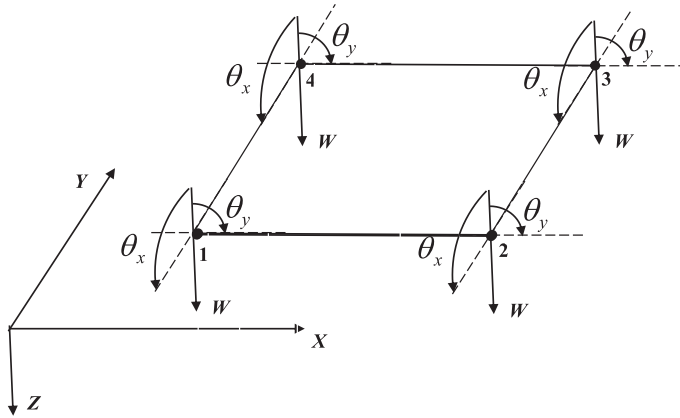
Figure 2. Co-ordinates and nodal points for the rectangular plate element 'ACM'.

$$[D] = \begin{bmatrix} D11 & D12 & 0 \\ D12 & D22 & 0 \\ 0 & 0 & D33 \end{bmatrix} \text{ is the usual constitutive matrix}$$

$$D11 = D22 = \frac{E}{\left(1 - v^2\right)}; D12 = \frac{v.E}{\left(1 - v^2\right)}; D33 = \frac{E}{2(1 + v)}$$

For [A] and $[K_0]$, see Appendices *A* and *B*.

At the end of the state determination, the two additional middle dofs are condensed out. The evaluation of the integral in Equation (8b) follows the approach of Melosh and Belarbi (2006) using an exact and nonreduced analytical integration. Such an approach resolves numerical problems associated with geometrical distortions of the element.

2.2. Rectangular plate element 'ACM'

The displacement fields of the **ACM** element (Figure 2) are given by the following expressions:

$$W(x, y) = a_1 + a_2 x + a_3 y + a_4 x^2 + a_5 xy + a_6 y^2 + a_7 x^3 + a_8 x^2 y + a_9 xy^2 + a_{10} y^3 + a_{11} x^3 y + a_{12} xy^3$$

$$\theta_x = -\left(a3 + a_5 x + 2 a_6 y + a_8 x^2 + 2a_9 xy + 3 a_{10} y^2 + a_{11} x^3 + 3 a_{12} xy^2\right) \quad (10)$$

$$\theta_y = a_2 + 2a_4 x + a_5 y + 3a_7 x^2 + 2a_8 xy + a_9 y^2 + 3 a_{11} x^2 y + a_{12} y^3$$
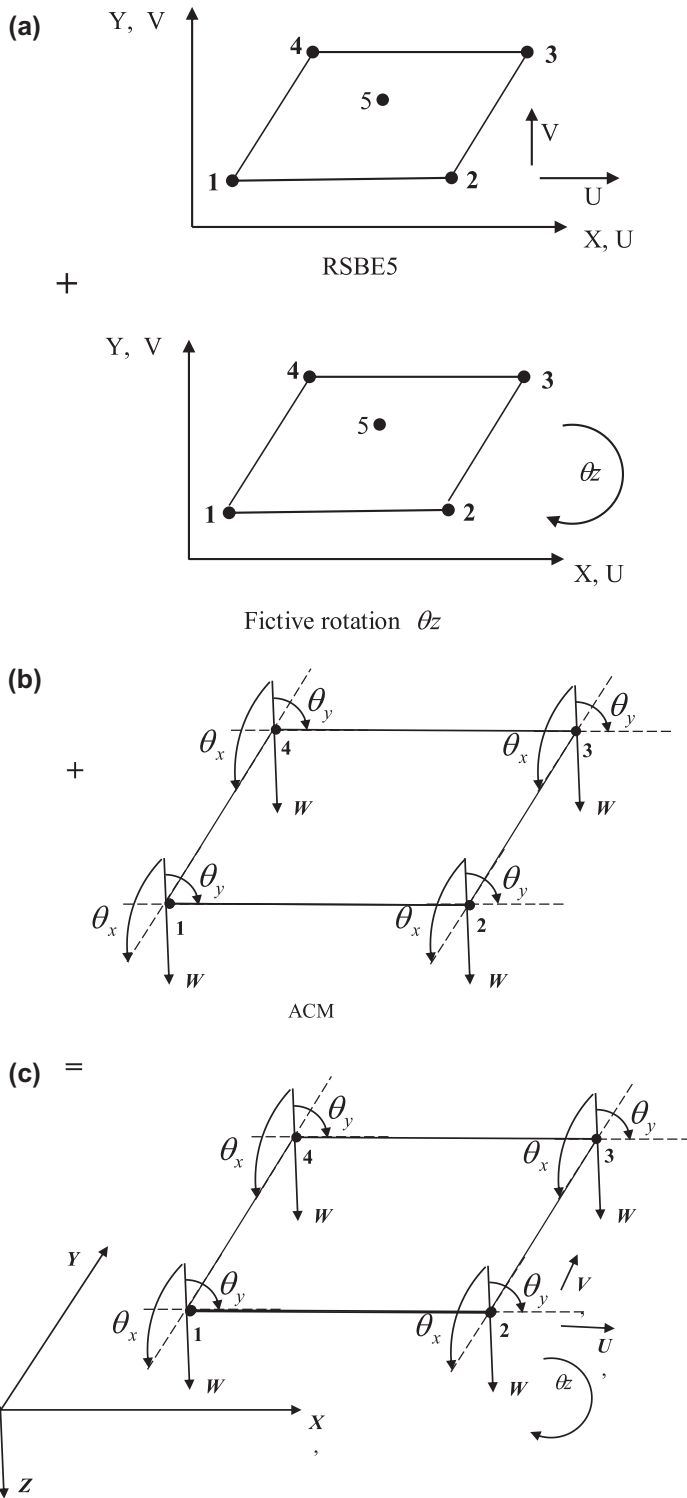
Figure 3. The shell element ACM_RSBE5.

(a)

Rigid diaphragm

(b)

Data:

$L=6$; $R=3m$; $h = 0,03m$; $E = 3 \times 10^{10}$ Pa ; $\nu = 0,3$

Symmetry conditions:

$$W = \theta_Y = \theta_X = 0 \quad \text{at} \quad AB$$
$$V = \theta_X = \theta_Z = 0 \quad \text{at} \quad BC$$
$$U = \theta_Y = \theta_Z = 0 \quad \text{at} \quad CD$$

Boundary conditions:

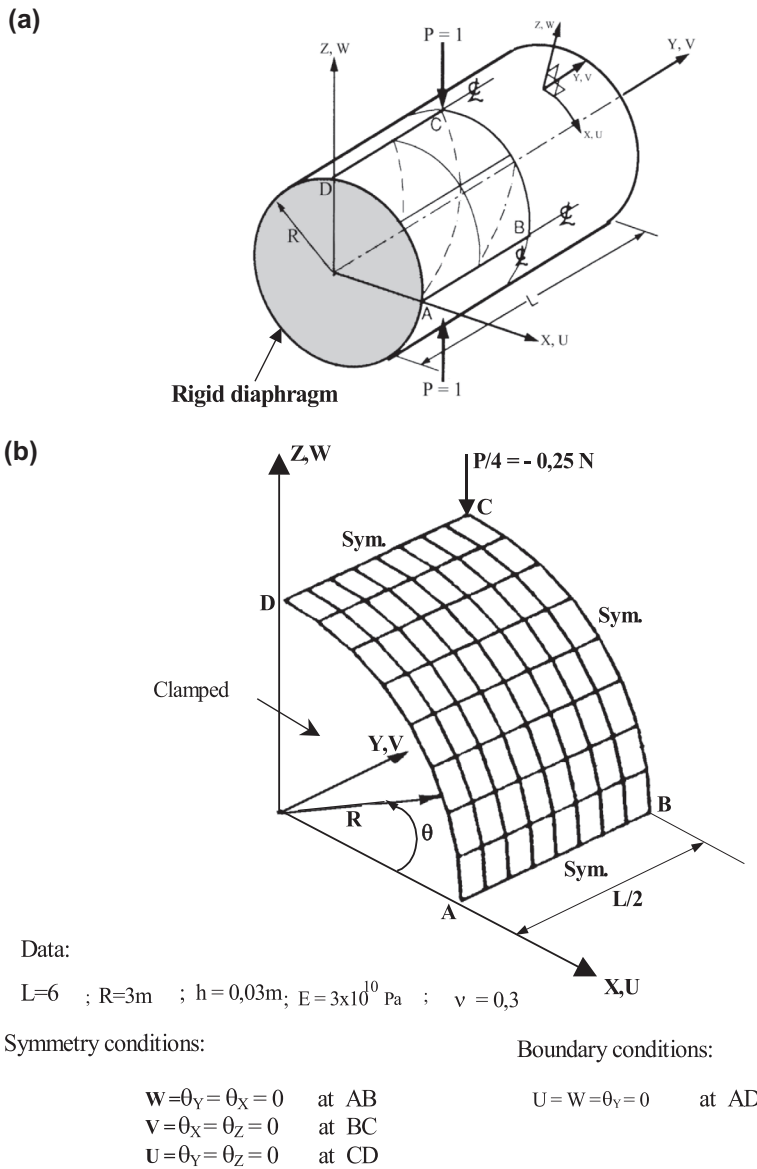$$U = W = \theta_Y = 0 \quad \text{at} \quad AD$$

Figure 4. Clamped cylindrical shell.

Table 1. Clamped cylindrical shell, convergence of W_C (normalised values).

	Displacement W_c at point C					
Meshes	ACM_RSBE5	ACM-SBQ4	HEX20	SHB8PS	RESS	Solution time (Sec) ACM_RSBE5
4 × 4	0.649	0.618	0.140	0.387	0.112	0.10000
6 × 6	0.842	0.821	0.328			0.17999
8 × 8	0.955	0.904	0.523	0.754	0.59	0.26999
20 × 4	0.984	0.956	0.675			0.28845
16 × 16				0.94	0.933	
Analytical solution	164.24 (1.00 Normalised results)					

Table 2. Clamped cylindrical shell, convergence of V_D.

Meshes	Displacement V_D at point D	
	ACM_RSBE5	ACM-SBQ4
4×4	6.206	6.153
6×6	4.837	4.809
8×8	4.521	4.274
20×4	4.179	4.192
Analytical solution	4.11	
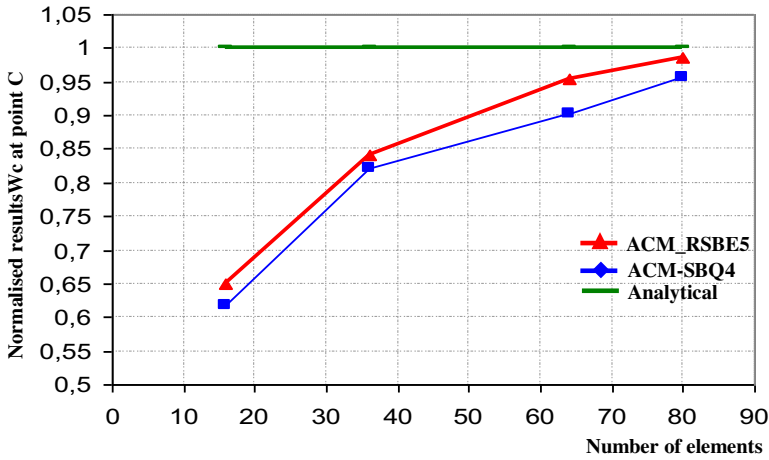
Figure 5. Convergence curve for the deflection W_c at point C.
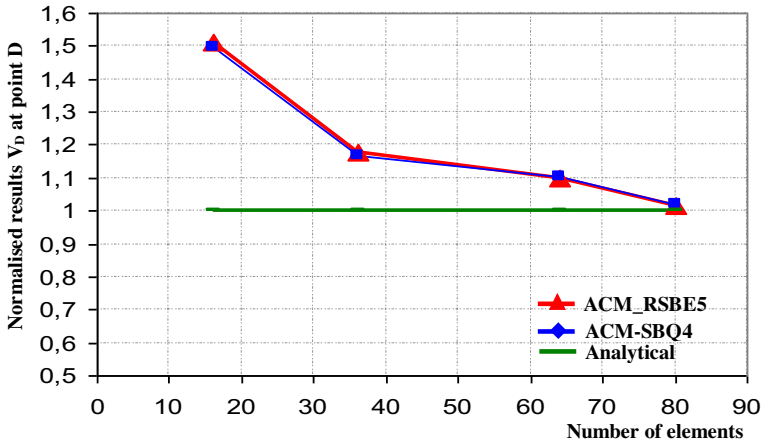
Figure 6. Convergence curve for the deflection V_D at point D.

The shell element **ACM_RSBE5** (Figure 3 (c)) is obtained by superposition of the two elements RSBE5 and ACM in the following manner:

$$(a) + (b) = (c)$$

3. Numerical tests

The performance of the formulated flat shell element is evaluated using the following popular test problems:

3.1. Clamped cylindrical shell

In this test problem, a clamped cylindrical shell (Figure 4 (a)) is evaluated. This test of thin shells ($R/h = 100$) is considered by many researchers as a severe test. It makes it possible to examine the aptitude of shell elements to simulate complicated membrane state problems dominated by bending. The dimensions, material properties and loading conditions are shown in Figure 4. Due to symmetry, only 1/8 of the shell (region ABCD) is considered in the finite-element idealisation (Figure 4 (b)).

The results obtained for different meshes for both, the proposed ACM_RSBE5 and the ACM_SBQ4 of Belarbi (2000), are presented in Tables 1 and 2.

The numerical results are compared to the analytical solution based on thin shell theories ($R/h = 100$), and given below by Flugge and Fosberge (1966) and Lindberg, Olson, and Cowper (1969):

$W_C = -W_C\, Eh/p = 164.24$ deflection under load P at point C only.

$V_D = -V_D\, Eh/p = 4.11$ deflection in the Y direction.

Table 1 also summarises the solution time used in the analysis of the clamped cylindrical shell with different meshes. The processor machine used has the following properties: Intel(R) Core(TM) i3–2330 M CPU@2.2 GHZ RAM: 4.00Go

The results obtained by the present element ACM_RSBE5 for the vertical displacement at point C (normalised values) are slightly better than those given by the element ACM-SBQ4, and much better than those of the hexahedral element HEX20, the standard full-integration solid element reported in Abed-Meraim, Trinh, and Combescure (2013). It also performs better than the six-node solid–shell element SHB6 (Abed-Meraim, Trinh, & Combescure, 2012), and the night-node solid–shell element SHB8PS (Abed-Meraim & Combescure, 2007) (Table 1). It performs relatively better than the widely used Reduced integration Enhanced strain Solid-Shell (RESS) element developed by Alves de Sousa et al. (2005) (Table 1). It significantly converges more rapidly than both, the standard prismatic elements PRI15 and the shell prismatic element SHB15 developed by Abed-Meraim et al. (2013), for example, for meshes (10 × 10) the results for these elements are 0.625 and 0.646, respectively, but for the ACM_RSBE5 is 0.955 for a mesh of 8 × 8 elements only. Even when compared with higher order elements, such as the 20-node solid–shell element SHB20 developed by Abed-Meraim et al. (2013), its performance is relatively good (0.955 as opposed to 0.979 for a mesh of 8 × 8).
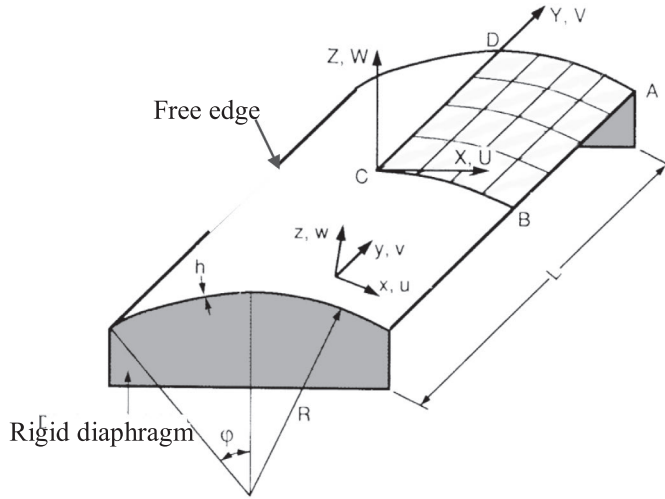
Data:

$L = 6$ m ; $R = 3$ m ; $h = 0,03$ m ; $\varphi = 40°$

$E = 3 \times 10^{10}$ Pa ; $\nu = 0$; $f_z = -0,625 \times 10^4$ Pa

Boundary conditions:

$U = W = \theta_Y = 0$ for AD

Symmetry conditions:

$U = \theta_Y = \theta_Z = 0$ for CD

$V = \theta_X = \theta_Z = 0$ for CB

Reference value (Deep Shell Theory):

$W_B = -3,61$ cm ; $W_C = 0,541$ cm

Analytical solution (Shallow Shell theory):

$W_B = -3,703$ cm ; $W_C = 0,525$ cm

$U_B = -1,965$ cm ; $V_A = -0,1513$ cm

Figure 7. Scordelis-Lo roof.
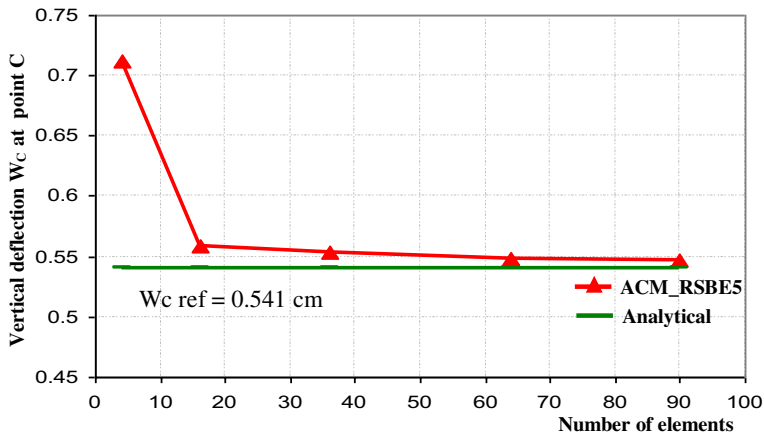
Figure 8. Convergence curve for the deflection W_c at point *C* Scordelis-Lo roof.
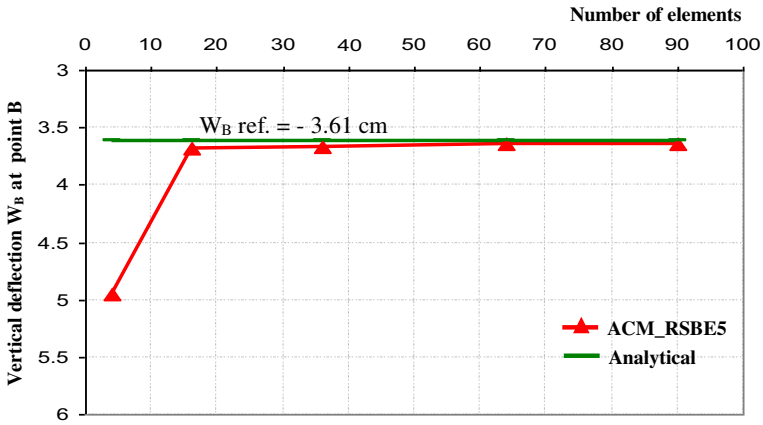
Figure 9. Convergence curve for the deflection WB at point B for Scordelis-Lo roof.
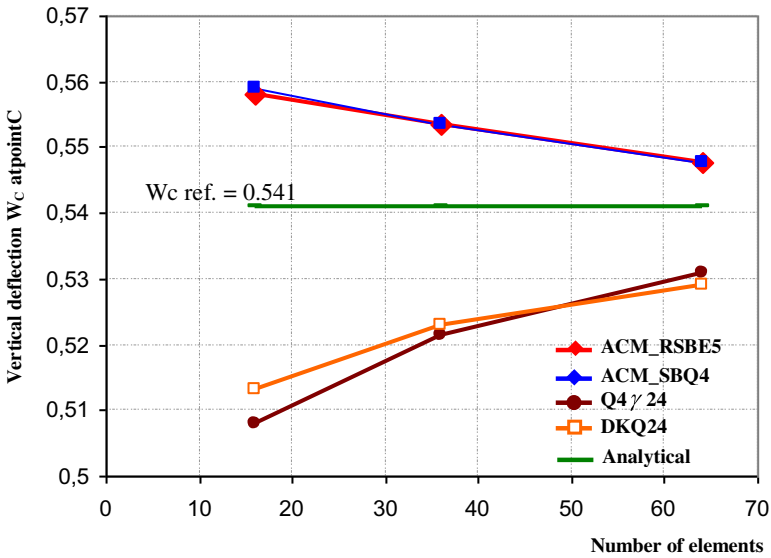
Figure 10. Convergence curve for the deflection W_c at point C for Scordelis-Lo roof.

The results obtained for both deflections W_C and V_D for the refined mesh (20×4) of the proposed element are in good agreement with the analytical solution.

Figures 5 and 6 show the convergence curves for the results obtained from elements **ACM_RSBE5** and ACM-SBQ4 for the deflections at points C and D. From the above figures, it is concluded that the **ACM_RSBE5** has a good convergence rate.

Figure 11. Convergence curve for the deflection WB at point B for Scordelis-Lo roof.

Data : Free edge

L=10,35 m ; R=4,953 m ; E=10,5 10^6 Pa ; v=0,3125
F_1=100 KN; h_1=0,094 m; F_2=0,1 KN ; h_2=0,01548 m

Figure 12. Pinched cylinder with free edges.

Table 3. Pinched cylinder with free edges, convergence of W_C.
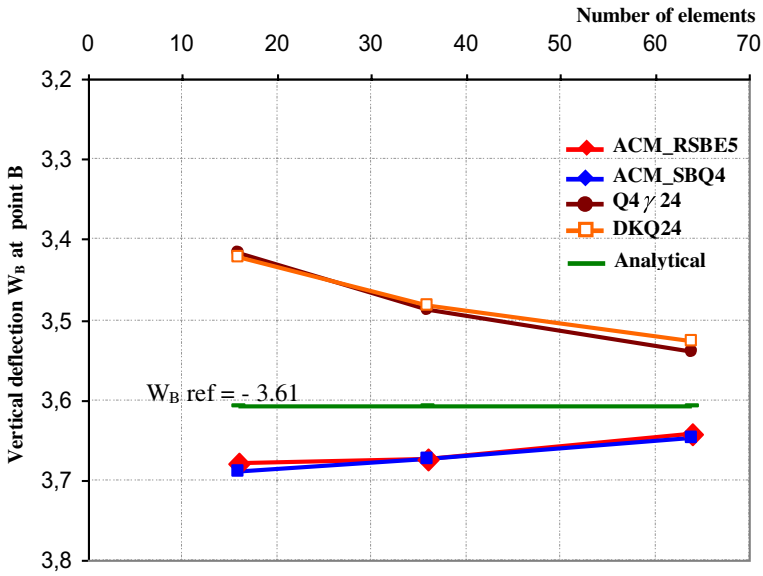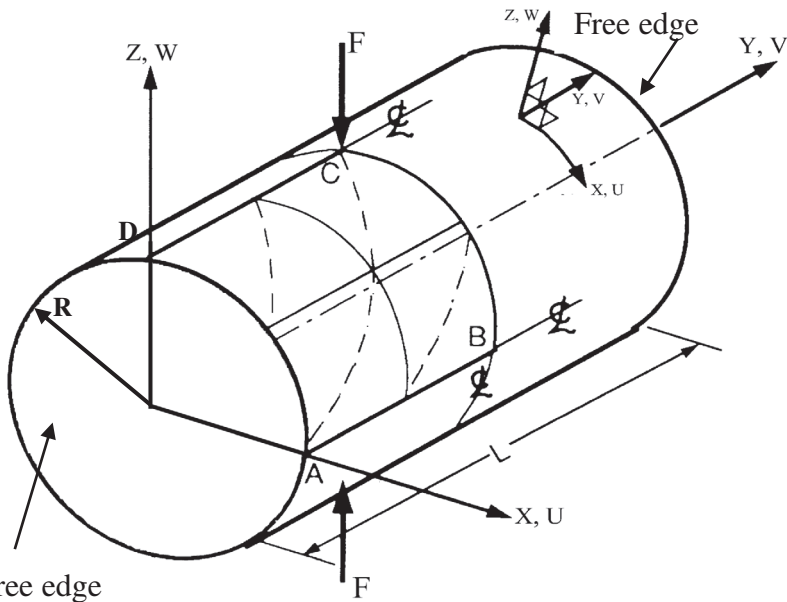
Meshes	W_C					Solution time (seconds) ACM_RSBE5
	[Bog 67) [29]	[CAN 68] with RBM [30]	[CAN 68] without RBM [30]	ACM_SBQ4 [19]	ACM_ RSBE5	
1×1	0.0025	–	–	0.0860	0.08763	0.006999
1×3	0.1026	0.0297	0.0009	0.1041	0.1060	0.016999
1×4	0.1087	–	–	–	0.1100	0.026000
1×5	–	0.0769	0.0021	0.1090	0.1116	0.043998
1×7	–	0.0987	0.0035	0.1102	0.1129	0.049998
1×8	–	–	–	–	0.1132	0.052000
1×9	–	0.1057	0.0051	0.1115	0.1134	0.054000
Exact solution		0.1139				

Note: Case 1: $P_1 = 100$; $h_1 = 0094$ m; $L = 10, 35$ m; $R = 4953$ m; $E = 10, 5 \times 10^6$; $v = 0, 3125$.

Table 4. Pinched cylinder with free edges, convergence of W_C.

Meshes	W_C					Solution time (seconds) for ACM_RSBE5
	[ASH 72] [4]	[CAN 68] [30]	[SAB 72] [23]	ACM_SBQ4 [19]	ACM_ RSBE5	
1×1	0.02301	0.00001	0.00001	0.01922	0.0196	0.0000
1×3	0.02302	0.00001	0.00001	0.02302	0.02343	0.00999
1×4	0.02403	0.00074	0.00063	–	–	
1×5	–	–	–	0.02387	–	
1×7	–	–	–	0.02418	–	
2×4	0.02409	0.00070	0.00064	–	–	
3×4	0.02414	0.00068	0.00065	–	–	
Exact solution		0.02439				

Note: Case 2: $P_2 = 0, 1$; $h_2 = 0, 01548$ m; $L = 10, 35$ m; $R = 4953$ m; $E = 10, 5 \times 10^6$; $v = 0, 3125$.
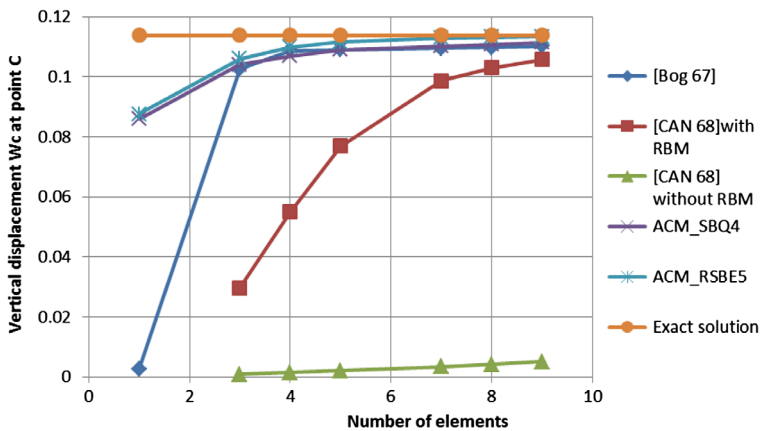
Figure 13. Convergence curve for the deflection W_c at point C for ACM_RSBE5 element and other quadrilateral shell elements, pinched cylinder with free edges, case 1.
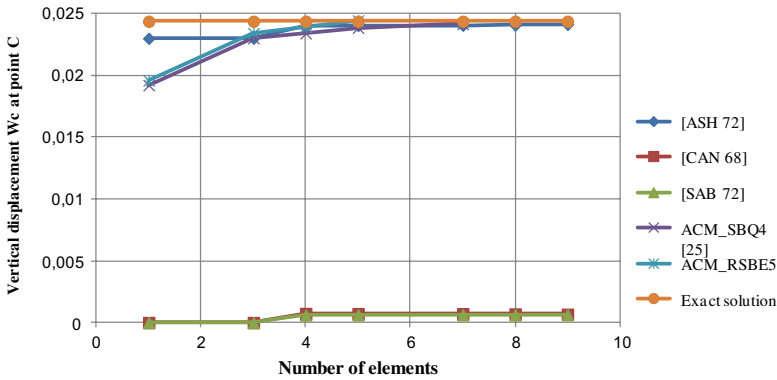
Figure 14. Convergence curve for the deflection W_c at point C for ACM_RSBE5 element and other quadrilateral shell elements, pinched cylinder with free edges, case 2.

3.2. Scordelis-Lo roof

In the next test problem, the Scordelis-Lo (1969) roof is considered. The roof structure has the geometry shown in Figure 7. The straight edges are free, while the curved edges are supported on rigid diaphragms along their plane. The geometry and material properties are given in Figure 7. Considering the symmetry of the problem, only one quarter of the roof is analysed (part ABCD). The results obtained using the proposed element **ACM_RSBE5** are compared to the reference values based on the deep shell theory.

The analytical solution based on the shallow shell theory is given by Scordelis and Lo (1969), which is slightly different from the deep shell theory. The convergence curves are presented in Figures 8 and 9 for the vertical displacement at the mid-point B of the free edge and the centre C of the roof.

The results are also compared to several other quadrilateral shell elements, namely Q4γ24, DKQ24 presented by Batoz and Dhatt (1992) and ACM-SBQ4 developed by Belarbi (2000). Figures 8–11 show the convergence curve for the deflections W_c at point C and W_B at point B obtained from the quadrilateral shell elements cited above.

The above results confirm the good convergence of the new formulated shell element **ACM_RSBE5.**

3.3. Pinched cylinder with free edges

The pinched cylinder shown in Figure 12 is one of the most common examples used in the literature to test shell elements. Indeed, since 1967 this example served as a test problem to assess the performance of new axisymmetric shell elements regarding the rapidity of convergence and especially the representation of rigid body modes. By reason of symmetry, only one-eighth of the cylinder is modelled.
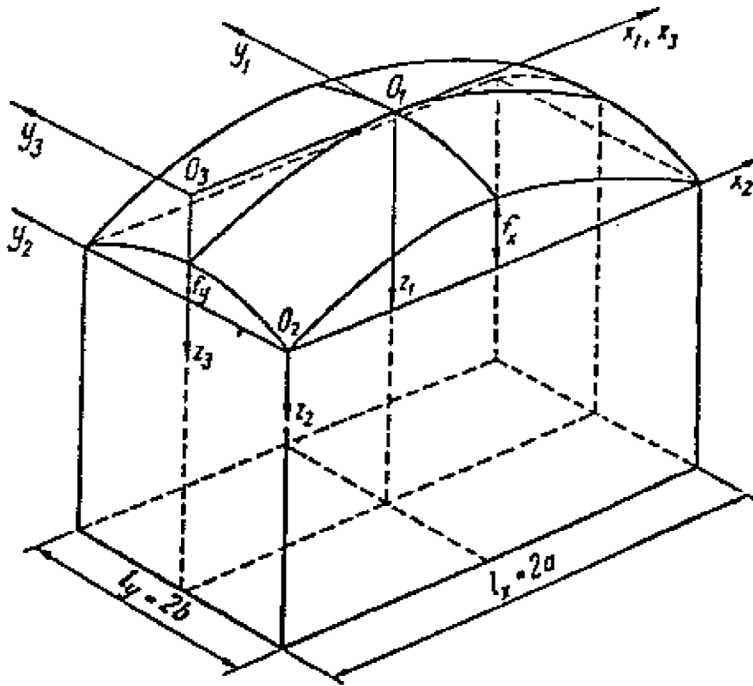
Figure 15. Elliptic paraboloid rectangular on plan.
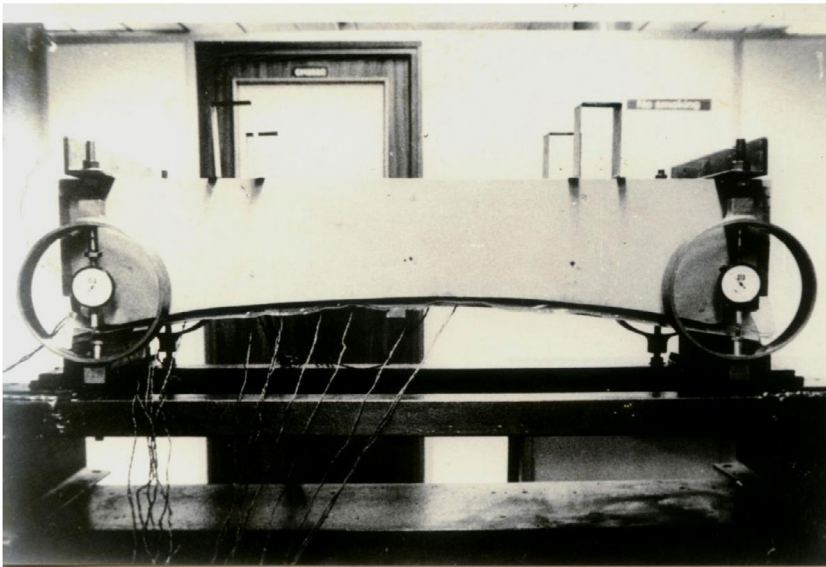
Figure 16. Elliptical paraboloid shell undergoing the experimental test.

The symmetry conditions are imposed along AB, AD and DC (Figure 12). Two cases of cylinder thickness and applied loads are considered (h_1, F_1 and h_2, F_2).
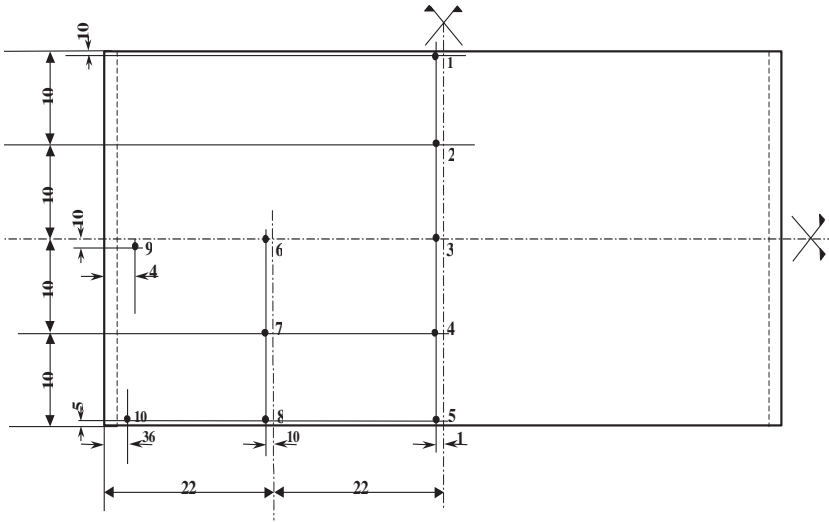
Figure 17. Dial gauge positions; (distance in mm).

One-eighth of the cylinder is modelled with different meshes, and the normal displacement W_C at point C is calculated. The convergence of the new element **ACM_RSBE5** is compared with the analytical solution (deep shells theory) and with other elements available in the literature; these are models: BOG (Bogner, Fox, & Schmit, 1967); CAN68 (Cantin & Clough, 1968); ASH72 (Ashwell & Sabir, 1972); and SAB72 (Sabir & Lock, 1972). The results obtained are presented in Tables 3 and 4, and the convergence curves for different elements are shown in Figures 13 and 14.

The results obtained and presented in Tables 3 and 4 and Figures 13 and 14 confirm the excellent performance of the formulated element ACM_RSBE5. The ACM_RSBE5 converges to deep shell solutions (to $W_C = -0.1139$ m for $h = 0.094$ m and $F = 100$ and from $W_C = -0.02439$ m $h = 0.01548$ m) with only a few elements (9 elements for the first case and 3 elements for the second case), contrarily to the other elements and slightly better than ACM_SBQ4.

4. Experimental investigation

A correlation study with an experimentally tested shell structure is conducted. The shell is assumed to be constructed from a perfectly elastic material. Tests on full-scale shell structures are scarce due to the associated high cost, hence the experimental work described in this study is for a small-scale specimen. The test details are described next.

4.1. Description of the elliptical paraboloid shell model (Figure 15)

The equation for the surface is written in the following manner as discussed by Beles and Soare (1975):

$$Z_1 = 4f_x \frac{x^2}{l_x^2} + 4f_y \frac{y^2}{l_y^2}$$

(11a)

Table 5. Vertical displacements **W** (mm) under different applied loadings.

	Points	3	4	5	6	7	8
Case a Load = 25 × 10 N/mm	ACM_RSBE5	0.24	0.40	2.01	0.16	0.25	0.41
	Exp.work	0.19	0.31	1.67	0.13	0.18	0.30
Case b Load = 50 × 10 N/mm	ACM_ RSBE5	0.48	0.80	4.02	0.32	0.50	0.82
	Exp.work	0.49	0.80	3.10	0.33	0.47	0.85
Case c Load = 75 × 10 N/mm	ACM_ RSBE5	0.72	1.20	6.03	0.48	0.75	1.23
	Exp.work	0.66	1.09	5.20	0.43	0.63	1.15
Case d Load = 100 × 10 N/mm	ACM_ RSBE5	0.96	1.60	8.02	0.65	1.00	1.64
	Exp.work	1.04	1.70	7.70	0.68	1.00	1.90

$$Z_2 = 4f_x \frac{x(x - l_x)}{l_x^2} + 4f_y \frac{y(y - l_y)}{l_y^2} \tag{11b}$$

$$Z_3 = f_x \left(\frac{2x}{l_x} - 1 \right)^2 + 4f_y \frac{y^2}{l_y^2} \tag{11c}$$

The elliptical shape specimen is made of an aluminium alloy and has a constant thickness of 2 mm with a rectangular projection of 880 mm by 400 mm (Figure 16). The material properties used are the modulus of elasticity $E = 70{,}000$ N/mm^2, the Poisson ratio $v = 0.33$. The shell is free along the long edges, and fixed on a wooden support along the short edges. Due to the double symmetry in geometry and loading, the measuring points are located on one quarter of the area of the model, at the eight points shown in Figure 17.

Eight deflections gauges capable of measuring displacements perpendicular to the surface of the shell are located under the shell. A further two deflection gauges are mounted to check for symmetry (Figure 17).

4.2. Loading

A uniform normal pressure is applied by covering the shell top surface with a pneumatic pressure bag. Four different values of loading are applied, 10, 20, 30 and 40 cm of water (in which 1 cm of water = 0.0142233 lb/ in^2 equivalent to 2.5×10^{-3} N/mm^2).

4.3 Numerical and experimental results

A mesh of 16 × 8 elements is used for the numerical analysis. The experimental and analytically computed vertical deflections for the different loading levels are presented in Table 5.

4.4. Comparison between theoretical and experimental results

In elastic analysis, as the loading was doubled, the deflections were doubled. This was not the case in the experimental work. This is due to a few points which could be explained as follows:

One of the main problems with the experiment was the lack of uniformity of the distributed load. The air-filled bag did not evenly distribute the pressure because loads measured at the four corners were found to be slightly different.

A further probable cause of inaccuracy was the positioning of the deflection gauges. The problem was to ensure that the gauges were perpendicular to the shell surface. Although this was easy to achieve in the central position (since it is horizontal), this was not so easily achieved near the edges where the shell surface is considerably angled.

In addition to the various experimental inaccuracies, in the theoretical analysis nondeflecting support conditions are assumed, which is not strictly the case in the experiments.

Finally, differences may results from other considerations. However, in general the results obtained from the finite-element analysis are in reasonable agreement with those measured experimentally.

5. Conclusion

A new strain-based element denoted ACM_RSBE5 is proposed. The element combines the new RSBE5 strain-based membrane model with the classical ACM plate model. A series of test problems were conducted to evaluate the efficiency of the element compared to other elements in the literature. The results obtained confirmed the fast convergence rate of the element. Further, a correlation study with an experimentally tested aluminium shell structure confirmed the accuracy of the proposed element, in particular in predicting the displacements of the inside points. The proposed element has the advantage of being simple in form and uses only the five essential degrees of freedom. Further, it can be used for the analysis of thin shell structures, even those with complex geometries. The current formulation is for linear analysis, but extension to account for both geometric and material nonlinearities is the subject of an ongoing investigation that will be published in future work.

Notations

a_i	Constants in displacement fields
[A]	Transformation matrix
[D]	Rigidity matrix
E, v	Young's modulus and Poisson's ratio, respectively
H	Shell thickness

$[K_e]$	Stiffness matrix
L	Shell length
$[Q]$	Strain matrix
R	Radius of the shell
U, V	In plane displacement in x and y, respectively
W	Normal displacement
X, Y	Cartesian coordinates
θ_x, θ_y and θ_z	rotations about x, y and z axes respectively
$\varepsilon_x, \varepsilon y$	Direct strains in the x and y directions
γ_{xy}	Membrane shear strain

Disclosure statement

No potential conflict of interest was reported by the authors.

References

Abed-Meraim, F., & Combescure, A. (2009). An improved assumed strain solidâ shell element formulation with physical stabilization for geometric non-linear applications and elasticâ plastic stability analysis. *International Journal for Numerical Methods in Engineering, 80*, 1640–1686.

Abed-Meraim, F., & Combescure, A. (2007). A physically stabilized and locking-free formulation of the SHB8PS solid-shell element. *European Journal of Computational Mechanics, 16*, 1037–1072.

Abed-Meraim, F., Trinh, V., & Combescure, A. (2012). Assumed strain solid–shell formulation for the six-node finite element SHB6: Evaluation on non-linear benchmark problems. *European Journal of Computational Mechanics, 21*, 52–71.

Abed-Meraim, F., Trinh, V., & Combescure, A. (2013). New quadratic solid–shell elements and their evaluation on linear benchmark problems. *Computing, 95*, 373–394.

Adini, A., & Clough, R. W. (1961). *Analysis of plate bending by the finite element method* (Report to the Nat. Sci. Found., G 7337), Arlington, TX, USA.

Alves de Sousa, R. J., Cardoso, R. P. R., Fontes Valente, R. A., Yoon, J. W., Grácio, J. J., & Natal Jorge, R. M. N. (2005). A new one-point quadrature enhanced assumed strain (EAS) solid-shell element with multiple integration points along thickness: Part I – geometrically linear applications. *International Journal for Numerical Methods in Engineering, 62*, 952–977.

Ashwell, D. G., & Sabir, A. B. (1972). A new cylindrical shell finite element based on simple independent strain functions. *International Journal of Mechanical Sciences, 14*, 171–183.

Bathe, K. J., & Wilson, E. L. (1976). *Numerical methods in finite element analysis*. Englewood Cliffs, NJ: Prentice Hall.

Batoz, J. L., & Dhatt, G. (1992). *Modélisation des structures par éléments finis*, (Vol. 3). Coques, Ed. Paris: Hermès.

Belarbi, M. T. (2000). *Développement de nouveaux éléments finis basés sur le modèle en déformation. Application linéaire et non linéaire* [Development of new finite elements based on the strain model: Application to linear and nonlinear problems] (Thèse de Doctorat d'état). Université de Constantine, Algérie.

Beles, A. A., & Soare, M. V. (1975). Elliptic and hyperbolic paraboloidal shells used in construction. *Bucharest* (pp. 145–146). London: Editura Academiei. S.P. Christie.

Bogner, F. K., Fox, R. L., & Schmit, L. A. (1967). A cylindrical shell discrete element. *AIAA Journal, 5*, 745–750.

Cantin, G., & Clough, R. W. (1968). A curved, cylindrical-shell, finite element. *AIAA Journal, 6*, 1057–1062.

Cardoso, R. P. R., Yoon, J. W., & Valente, R. A. (2006). A new approach to reduce membrane and transverse shear locking for one-point quadrature shell elements: Linear formulation. *International Journal for Numerical Methods in Engineering, 66*, 214–249.

Cardoso, R. P., Yoon, J. W., Mahardika, M., Choudhry, S., Alves de Sousa, R. J., & Fontes Valente, R. A. (2008). Enhanced assumed strain (EAS) and assumed natural strain (ANS) methods for one-point quadrature solid-shell elements. *International Journal for Numerical Methods in Engineering, 75*, 156–187.

Corner, J. J., Brebbia, C. (1967). Stiffness matrix for shallow rectangular shell element. *Journal of Engineering Mechanics (ASCE), 93*, 43–65.

Djoudi, M. S., & Bahai, H. (2003). A shallow shell finite element for the linear and non-linear analysis of cylindrical shells. *Engineering Structures, 25*, 769–778.

Djoudi, M. S., & Bahai, H. (2004). A cylindrical strain-based shell element for vibration analysis of shell structures. *Finite Elements in Analysis and Design, 40*, 1947–1961.

Flugge, W., & Fosberge, K. (1966). Point load on shallow elliptic paraboloid. *Journal of Applied Mechanics, 33*, 575–585.

Hamadi, D. (2006). *Analysis of structures by non-conforming finite elements* (PhD thessis). Civil Engineering Department, Biskra University, Algeria, pp. 130.

Hartmann, F., & Kats, C. (2007). *Structural Analysis with finite element methods*. (2nd ed.). Berlin: Springer-Verlag.

Jones, R. E., Strome, D. R. (1966). Direct stiffness method analysis of shells of revolution utilizing curved elements. *AIAA Journal, 4*, 1519–1525.

Kulikov, G. M., & Plotnikova, S. V. (2010). A family of ANS four-node exact geometry shell elements in general convected curvilinear coordinates. *International Journal for Numerical Methods in Engineering, 83*, 1367–1406.

Melosh, D., & Belarbi, M. T. (2006). Basis for derivation of matrices for the direct stiffness method. *AIAA Journal, 7*, 525–549.

Melosh, R. J. (1963). Basis of derivation of matrices for the direct stiffness method. *Journal of AIAA, 1*, 1631–1637.

Mousa, A. I. (1992). *Triangular finite element for analysis of spherical shell structures* (UWCC Publications, Internal Report). Cardiff: University of Wales, college Cardiff.

Mousa, A. I., & EL Naggar, M. H. (2007). Shallow spherical shell rectangular finite element for analysis of cross shaped shell roof. *Electronic Journal of Structural Engineering, 7*, 769–778.

Mousa, A. I., & Sabir, A. B. (1994). Finite element analysis of fluted conical shell roof structures. *Computational Structural Engineering in Practice, Civil Comp. press-* ISRN O-948 748- *30x*, 173–181.

Reese, S. (2007). A large deformation solid-shell concept based on reduced integration with hourglass stabilization. *International Journal for Numerical Methods in Engineering, 69*, 1671–1716.

Sabir, A. B. (1997). *Strain based shallow spherical shell element*. Proc. Int. Conf on the Math. Finite elements and application, Brunel University, England.

Sabir, A. B., & Charchaechi, T. A. (1982). Curved rectangular and general quadrilateral shell finite elements for cylindrical shells. In J. R. Whiteman (Ed.), *The math of finite element and application* (pp. 231–239). London: Academic Press.

Sabir, A. B., & Djoudi, M. S. (1990). A shallow shell triangular finite element for the analysis of hyperbolic parabolic shell roof. *FEMCAD. Struct. Eng. and Optimization*, 49–54.

Sabir, A. B., & Djoudi, M. S. (1998). A shallow shell triangular finite element for the analysis of spherical shells. *Structural Analysis Journal*, 51–57.

Sabir, A. B., & Lock, A. C. (1972). A curved cylindrical shell finite element. *IJMS, 14*, 125–135.

Sabir, A. B., & Ramadhani, F. (1985). *A shallow shell finite element for general shell analysis.* Variation Method in Engineering, Proceedings of the 2nd International Conference, University of Southampton, England.

Schwarze, M., & Reese, S. (2009). A reduced integration solid-shell finite element based on the EAS and the ANS concept-geometrically linear problems. *International Journal for Numerical Methods in Engineering, 80*, 1322–1355.

Scordelis, A. C., & Lo, K. S. (1969). Computer analysis of cylindrical shells. *Journal of American Concrete Institute, 61*, 539–561.

Simo, J. C., & Rifai, M. S. (1990). A class of mixed assumed strain methods and the method of incompatible modes. *International Journal for Numerical Methods in Engineering, 29*, 1595–1638.

Zienkiewics, O. C. (1977). *The finite element method* (3rd ed.). London: McGraw Hill.

Zienkiewics, O. C., & Taylor, R. L. (2000). *The finite element method, Vol. solid mechanics* (5th ed.). Butterworth: Heinemann.

Appendix A

$$[A] = \begin{bmatrix}
1 & 0 & 0 & 0 & 0 & 0 & 0 & 0 & 0 & 0 \\
0 & 1 & 0 & 0 & 0 & 0 & 0 & 0 & 0 & 0 \\
1 & 0 & 0 & a & 0 & 0 & 0 & 0 & \frac{a^2}{2} & 0 \\
0 & 1 & a & 0 & \frac{-a^2(R+1)}{2} & 0 & 0 & \frac{a}{2} & 0 & \frac{-Ha^2}{2} \\
1 & 0 & -b & a & ab & 0 & \frac{-b^2(R+1)}{2} & \frac{b}{2} & \frac{a^2-Hb^2}{2} & 0 \\
0 & 1 & a & 0 & \frac{-a^2(R+1)}{2} & b & ab & \frac{a}{2} & 0 & \frac{b^2-Ha^2}{2} \\
1 & 0 & -b & 0 & 0 & 0 & \frac{-b^2(R+1)}{2} & \frac{b}{2} & \frac{-Hb^2}{2} & 0 \\
0 & 1 & 0 & 0 & 0 & b & 0 & 0 & 0 & \frac{b^2}{2} \\
1 & 0 & -\frac{b}{2} & \frac{a}{2} & \frac{ab}{4} & 0 & -\frac{b}{8}^2(R+1) & \frac{b}{4} & \frac{a^2-Hb^2}{8} & 0 \\
0 & 1 & \frac{a}{2} & 0 & -\frac{a}{8}^2(R+1) & \frac{b}{2} & \frac{ab}{4} & \frac{a}{4} & 0 & \frac{b^2-Ha^2}{8}
\end{bmatrix}$$

Appendix B

$$[K_0] = \begin{bmatrix}
0 & 0 & 0 & 0 & 0 & 0 & 0 & 0 & 0 & 0 \\
 & 0 & 0 & 0 & 0 & 0 & 0 & 0 & 0 & 0 \\
 & & 0 & 0 & 0 & 0 & 0 & 0 & 0 & 0 \\
 & & & H_1 & H_2 & H_3 & H_4 & 0 & H_5 & H_6 \\
 & & & & H_7 & H_8 & H_9 & H_{10} & H_{11} & H_{12} \\
 & & & & & H_{13} & H_{14} & 0 & H_{15} & H_{16} \\
 & & & & & & H_{17} & H_{18} & H_{19} & H_{20} \\
 & & & & & & & H_{21} & H_{22} & H_{23} \\
 & & & & & & & & H_{24} & H_{25} \\
 & & & & & & & & & H_{26}
\end{bmatrix}$$

$H_1 = abD_{11}$

$H_2 = \frac{1}{2}ab^2D_{11}$

$H_3 = abD_{12}$

$H_4 = \frac{1}{2}ba^2D_{12}$

$H_5 = \frac{1}{2}ba^2D_{11}$

$H_6 = \frac{1}{2}ab^2D_{12}$

$H_7 = \frac{1}{3}\left(ab^3D_{11} + ba^3R^2D_{33}\right)$

$H_8 = \frac{1}{2}ab^2D_{12}$

$H_9 = \frac{a^2b^2}{4}\left(R^2D_{33} + D_{12}\right)$

$H_{10} = -\frac{1}{2}Rba^2D_{33}$

$H_{11} = \frac{a^2b^2}{4}\left(RHD_{33} + D_{11}\right)$

$H_{12} = \frac{1}{3}\left(ab^3D_{12} + ba^3RHD_{33}\right)$

$H_{13} = abD_{22}$

$H_{14} = \frac{1}{2}ba^2D_{22}$

$H_{15} = \frac{1}{2}ba^2D_{12}$

$H_{16} = \frac{1}{2}ab^2D_{22}$

$H_{17} = \frac{1}{3}\left(ba^3D_{22} + ab^3R^2D_{33}\right)$

$H_{18} = -\frac{1}{2}ab^2RD_{33}$

$H_{19} = \frac{1}{3}\left(ba^3D_{12} + ab^3RHD_{33}\right)$

$H_{20} = \frac{a^2b^2}{4}\left(RHD_{33} + D_{22}\right)$

$H_{21} = abD_{33}$

$H_{22} = -\frac{1}{2}ab^2HD_{33}$

$H_{23} = -\frac{1}{2}ba^2HD_{33}$

$H_{24} = \frac{1}{3}\left(ab^3H^2D_{33} + ba^3D_{11}\right)$

$H_{25} = \frac{a^2b^2}{4}\left(H^2D_{33} + D_{12}\right)$

$H_{26} = \frac{1}{3}\left(ba^3H^2D_{33} + ab^3D_{22}\right)$

Where: $D11 = D22 = \frac{E}{\left(1-v^2\right)}; D12 = \frac{v.E}{\left(1-v^2\right)}; D33 = \frac{E}{2(1+v)}$

With: $H = \frac{2}{(1-v)}; R = \frac{2v}{(1-v)}$